ADVANCED MATERIALS
www.advmat.de

Locally Concentrated Deep Eutectic Liquids Electrolytes for Low-Polarization Aluminum Metal Batteries

Cheng Xu, Thomas Diemant, Xu Liu, and Stefano Passerini**

Low-cost and nontoxic deep eutectic liquid electrolytes (DELEs), such as $[AlCl_3]_{1.3}$[Urea] (AU), are promising for rechargeable non-aqueous aluminum metal batteries (AMBs). However, their high viscosity and sluggish ion transport at room temperature lead to high cell polarization and low specific capacity, limiting their practical application. Herein, non-solvating 1,2-difluorobenzene (dFBn) is proposed as a co-solvent of DELEs using AU as model to construct a locally concentrated deep eutectic liquid electrolyte (LC-DELE). dFBn effectively improves the fluidity and ion transport without affecting the ionic dynamics in the electrolyte. Moreover, dFBn also modifies the solid electrolyte interphase growing on the aluminum metal anodes and reduces the interfacial resistance. As a result, the lifespan of Al/Al cells is improved from 210 to 2000 h, and the cell polarization is reduced from 0.36 to 0.14 V at 1.0 mA cm^{-2}. The rate performance of Al-graphite cells is greatly improved with a polarization reduction of 0.15 and 0.74 V at 0.1 and 1 A g^{-1}, respectively. The initial discharge capacity of Al-sulfur cells is improved from 94 to 1640 mAh g^{-1}. This work provides a feasible solution to the high polarization of AMBs employing DELEs and a new path to high-performance low-cost AMBs.

1. Introduction

Non-aqueous rechargeable aluminum metal batteries (AMBs), in which the highly abundant, low-cost, and high-capacity (2980 mAh g^{-1} and 8040 mAh cm^{-3}) aluminum metal is used as the anode material, are promising candidates for the next-generation energy storage devices and have attracted increasing attention.[1,2] Electrolytes are important components of rechargeable metal batteries,[3] not only governing the transport of ionic charge carriers between the cathode and anode, but also affecting the electrochemical processes at the electrode/electrolyte interfaces.[4–6]

Currently, the state-of-the-art electrolyte for room-temperature rechargeable AMBs consists of aluminum chloride ($AlCl_3$) and 1-ethyl-3-methylimidazolium chloride ([EMIm]Cl) in a mole ratio of 1.3:1.[7,8] Due to the capability of reversible aluminum stripping/plating at room temperature via the conversion between $AlCl_4^-$ and $Al_2Cl_7^-$ (Equation (1)), this electrolyte has been widely used realizing high-performance AMBs with various different cathode materials, such as graphite,[9–11] transition metal chalcogenides,[12–16] Prussian blue analogues,[17] MXenes,[7,18–20] organic compounds,[21,22] and chalcogens.[23–27] However, the high cost of [EMIm]Cl greatly limits the development of AMBs.[28] To tackle the cost factor, deep eutectic liquid electrolytes (DELEs) formed via mixing of the Lewis acid $AlCl_3$ with a Lewis basic ligand like urea were proposed as alternative electrolytes,[29] in which the heterolytic cleavage of $AlCl_3$ leads to the generation of $AlCl_4^-$, $Al_2Cl_7^-$, and $[AlCl_2\cdot(ligand)_n]^+$.[30,31] With careful optimization of the mole ratio between $AlCl_3$ and the ligand to adjust the dynamic equilibrium of these ionic species in the electrolytes,[32,33] reversible stripping/plating of aluminum can be realized as described by Equations (1) and (2).[34]

$$4Al_2Cl_7^- + 3e^- \leftrightarrow Al + 7AlCl_4^- \quad (1)$$

$$2\left[AlCl_2\cdot(ligand)_2\right]^+ + 3e^- \leftrightarrow Al + AlCl_4^- + 4(ligand) \quad (2)$$

The replacement of [EMIm]Cl with the inexpensive Lewis basic ligands can effectively reduce the cost of the electrolyte. On the other hand, the strong coordination of urea toward Al^{3+} leads to significantly increased viscosity and decreased ionic conductivity,[35] resulting in severe cell polarization and low cathode materials utilization.[30,36]

The addition of low-viscosity co-solvents to DELEs can reduce the viscosity and improve the ionic conductivity,[37] which

C. Xu, T. Diemant, X. Liu, S. Passerini
Helmholtz Institute Ulm (HIU)
Helmholtzstraße 11, D-89081 Ulm, Germany
E-mail: xu.liu@kit.edu; stefano.passerini@kit.edu
C. Xu, T. Diemant, X. Liu, S. Passerini
Karlsruhe Institute of Technology (KIT)
P.O. Box 3640, D-76021 Karlsruhe, Germany
S. Passerini
Chemistry Department
Sapienza University
Piazzale A. Moro 5, Rome I-00185, Italy

The ORCID identification number(s) for the author(s) of this article can be found under https://doi.org/10.1002/adma.202400263

DOI: 10.1002/adma.202400263

has been validated to promote electrochemical performance of supercapacitors,[38] redox flow batteries,[39] and zinc metal batteries.[40] Nonetheless, the selection of organic solvents for $AlCl_3$-based DELEs is challenging.[41] First, co-solvents with strong solvation ability can affect the molar ratio of $AlCl_4^-$, $Al_2Cl_7^-$, and $[AlCl_2{\cdot}(ligand)_n]^+$ in DELEs, which is critical for Al stripping/plating. Second, $AlCl_3$ can react with the co-solvents due to its strong Lewis acidity. Recently, fluorinated aromatic compounds and ethers featured with unique non-solvating character emerged as a new class of co-solvents of high concentration electrolytes (HCEs) to construct locally concentrated electrolytes,[42–44] which effectively rescue the high viscosity and low conductivity of HCEs without affecting their local solvation.[45–49] In this context, these non-solvating compounds appear to be potential co-solvent candidates of DELEs for AMBs. To the best of our knowledge, the use of DELEs aided with non-solvating co-solvents as electrolytes for AMBs has not been reported yet.

Herein, a locally concentrated DELE (LC-DELE) is for the first time proposed for AMBs (i.e., Al-graphite and Al-S batteries). The DELE $[AlCl_3]_{1.3}[Urea]_1$ (AU) and the non-solvating (co-solvent) 1,2-difluorobenzene (dFBn) were selected as model compounds to investigate the physical properties of the resulting LC-DELE and their influence on the AMBs' electrochemical performance. The results demonstrate that introducing dFBn into AU effectively promotes the fluidity and ionic transport without affecting the ion dynamics in the electrolytes. Moreover, dFBn participates in the formation of the solid electrolyte/electrode interphase (SEI) on the aluminum metal anode (AMA), reducing the interfacial resistance. As a result, dFBn, as a co-solvent, effectively reduces the polarization of Al-graphite and Al-sulfur (Al-S) batteries. These results demonstrate that adding non-solvating co-solvents into DELEs is a feasible strategy enabling low-polarization AMBs.

2. Results and Discussion

2.1. Physicochemical Properties and Solvation Structure of the Electrolytes

In the first step, the physicochemical properties and solvation structure of LC-DELEs consisting of AU and dFBn were determined. For this purpose, different amounts of dFBn were added to AU, the resulting mixtures $[AlCl_3]_{1.3}[Urea]_1[dFBn]_x$ are in the following named as AUdF-x (x = 0.2, 0.4, 0.6). As displayed in Figure S1 (Supporting Information), AUdF-0.4 is a clear and homogeneous solution upon storage at room temperature. To evaluate the influence of dFBn on the fluidity of AU, the dynamic viscosity (μ) of the electrolytes at room temperature was calculated based on their density (ρ) and kinematic viscosity (ν) as described by the following equation:

$$\mu = \nu \times \rho \tag{3}$$

The kinematic viscosity was obtained by averaging three parallel experimental results (Table S1, Supporting Information). The calculated dynamic viscosity of the electrolytes is summarized in **Figure 1a**. Taken together, the addition of dFBn results in a significant viscosity's reduction (Figure 1a). For instance, the viscosities of AU and AUdF-0.6 are 316.4 and 25.9 mPa s, respectively. Figure 1b shows the ionic conductivity of the electrolytes at 20 °C. The dFBn-free sample (AU) has the lowest ionic conductivity of 0.5 mS cm^{-1}. With increasing dFBn concentration, a bell-shape trend with a maximum of 1.95 mS cm^{-1} for $x = 0.4$ is observed, due to the opposite effects of decreasing ionic charge carrier concentration and viscosity. These results demonstrate that the addition of dFBn with the suitable amount, e.g., x = 0.4, can simultaneously promote the fluidity and ionic transport of the electrolytes, which is desired for a lower cell polarization and better utilization of cathode material.

As mentioned, the dynamic equilibrium between the ionic species in the electrolytes is important for the electrochemical reactions of AMBs. Therefore, Raman spectra of dFBn, AU, and AUdF were recorded to track the changes of the ion–ion and ion–solvent interactions. The spectra of AU and AUdF were normalized to the peak of $AlCl_4^-$ at 350 cm^{-1}. The Raman spectra in the region of 250–500 and 950–1200 cm^{-1} are shown in Figure 1c,d, respectively. In Figure 1c, the peaks at 314 and 350 cm^{-1} can be assigned to the Al–Cl bond from $Al_2Cl_7^-$ and $AlCl_4^-$, respectively. The addition of dFBn into AU leads to the rise of a peak at 298 cm^{-1} corresponding to pure dFBn. More important, no noticeable change of peak position of relative intensity of the peaks of $AlCl_4^-$ and $Al_2Cl_7^-$ could be detected upon addition of dFBn. As shown in Figure 1d, the Raman peak at 1058 cm^{-1} originates from the C–N stretching vibration of urea species.[50] Its position and intensity normalized to the $AlCl_4^-$ peak at 350 cm^{-1} are not affected with the addition of dFBn.

Finally, the flashpoint of AU and AUdFs was tested to evaluate their flammability. No flash occurred during the test of these samples in the 25–250 °C temperature range, indicating their non-flammable character. Figure S2 (Supporting Information) presents the differential scanning calorimetry (DSC) and thermal gravimetric analysis (TGA) spectra of AU and AUdF-0.4. The results demonstrate that the addition of dFBn widens the liquidus range of the electrolyte. Also, AUdF-0.4 is thermally stable until dFBn starts to evaporate at 50 °C. These results demonstrate that dFBn as a non-solvating co-solvent for AU can effectively promote the fluidity and ionic transport without affecting its ion solvation and non-flammability. Since AUdF-0.4 (later simply named as AUdF) exhibits the highest ionic conductivity, it was selected as the model electrolyte.

2.2. Electrochemical Performance and Interfacial Properties of AMAs in AUdF

To investigate the effect of dFBn on AMAs' electrochemical properties, Al/Al symmetric cells employing AU and AUdF electrolytes were assembled and tested at 20 °C. **Figure 2a** displays the voltage profiles of the cells upon Al stripping/plating under various current densities, the corresponding average voltage for 5 stripping/plating cycles (positive value) at each current density are compared in Figure 2b. Both cells performed at current densities up to 1.0 mA cm^{-2}, but the AU-based cell showed a fast-increasing voltage when the current density was increased to 0.75 mA cm^{-2}. In contrast, the AUdF-based cell showed a steady voltage plateau even at 1.0 mA cm^{-2}. Moreover, this cell always

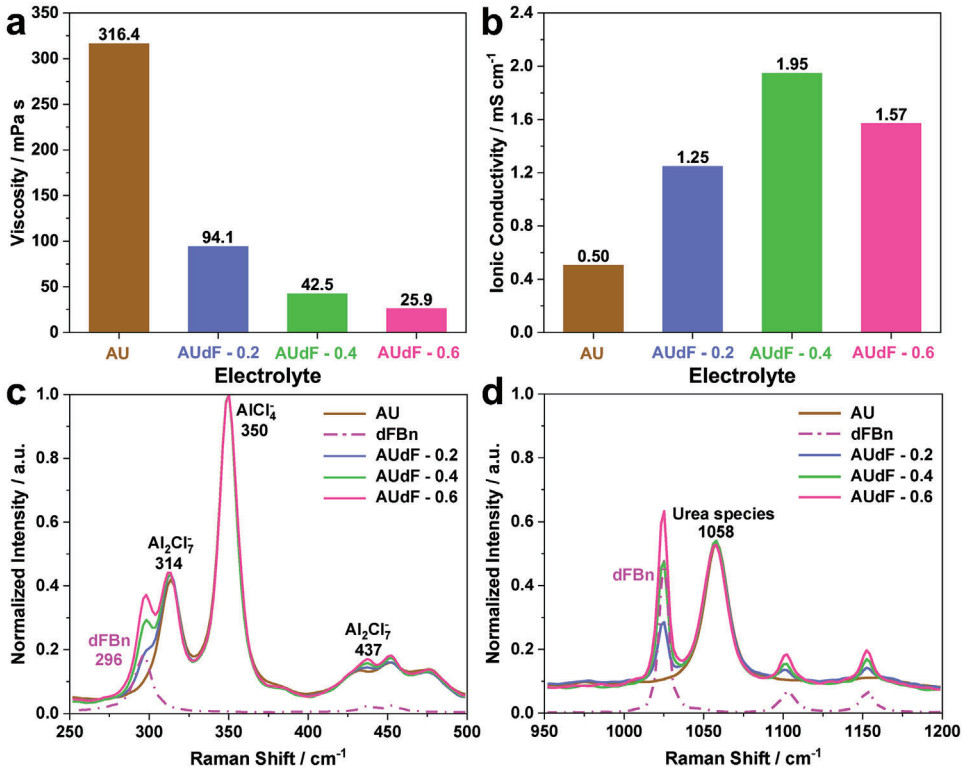

Figure 1. a) Dynamic viscosity of AU and AUdF-*x* at room temperature. b) Ionic conductivity of AU and AUdF-*x* at 20 °C. Raman spectra of AU, dFBn, and AUdF-*x* in the range of c) 250–500 cm^{-1} and d) 950–1200 cm^{-1}. The Raman spectra of AU and AUdF-*x* are normalized to the $AlCl_4^-$ peak at 350 cm^{-1}, while the Raman spectrum of dFBn is the original curve.

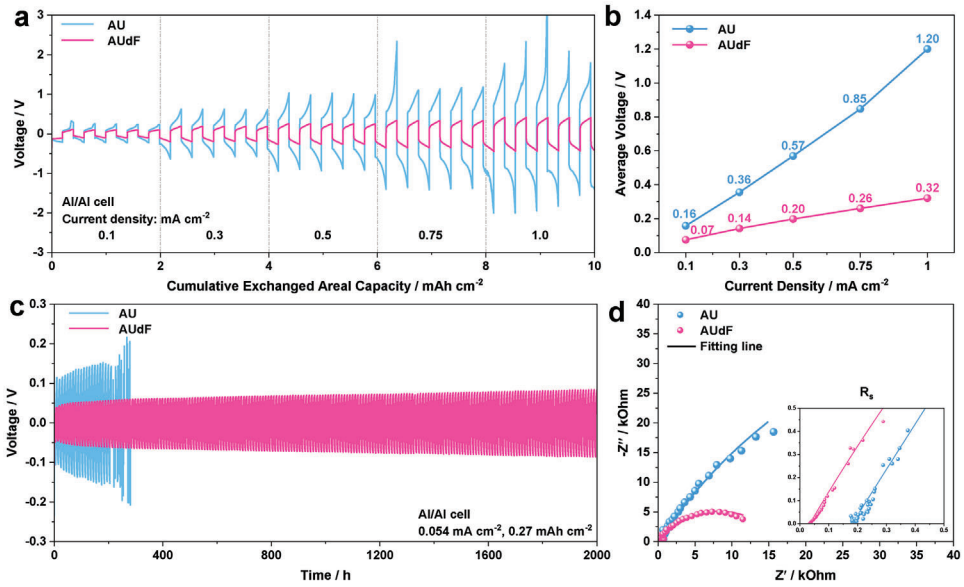

Figure 2. Electrochemical performance of Al/Al symmetric cells employing AU and AUdF-0.4 as electrolytes at 20 °C. a) Voltage evolution upon stripping/plating at different current densities from 0.1 to 1 mA cm^{-2} and b) the corresponding average voltage for five positive curves. c) Voltage evolution upon long-term stripping/plating cycles (5 h for each step) at 0.054 mA cm^{-2}. d) Nyquist plots extracted from EIS measurements after 15 cycles.

showed the lowest over-voltage at the end of each step, being 2–4 times lower than that of the AU-based cell.

The long-term cyclability of AMAs in the electrolytes was tested with symmetric Al/Al cells at a current density of 0.054 mA cm^{-2} and a cycled capacity of 0.27 mAh cm^{-2}. The voltage profile variation of both cells upon cycling is displayed in Figure 2c, while the profiles of a few selected cycles are shown in Figure S3 (Supporting Information). The over-voltage of the AU-based cell was obviously higher, with the average voltage growing from 80 mV at the 1st cycle to 104 mV at the 20th cycle (Figure S3a,b, Supporting Information). This cell incurred in a short circuit after cycling for 210 h (Figure S3b, Supporting Information). The Al/Al cell employing AUdF, instead, presented a stable cycling for 2000 h (Figure 2c) with its average voltage increasing from 36 mV to only 61 mV during cycling (Figure S3c, Supporting Information). The thoroughly reduced over-potential and improved cycling stability demonstrates the high compatibility of dFBn as a co-solvent of AU for high-rate and long-lifespan AMAs. For comparison, a non-fluorinated electrolyte employing dimethyl carbonate (DMC) as a co-solvent, i.e., $[AlCl_3]_{1.3}[Urea]_1[DMC]_{0.4}$, was also tested in Al/Al symmetric cell (Figure S4, Supporting Information). The huge polarization of the cell, up to 6 V, indicates that DMC does not support Al stripping/plating, i.e., not all aprotic co-solvents into deep eutectic liquids are appropriate.

Al/Cu cells were assembled to further explore the effect of dFBn on the Coulombic efficiency (CE) of Al stripping/plating. To increase the adhesion of the deposit on the substrate and decrease the nucleation barrier, carbon fiber-coated Cu electrodes (Figure S5, Supporting Information) were used as the working electrodes for the tests. As shown in Figure S6 (Supporting Information), the addition of dFBn into AU increased the CE from ≈80% to ≈88%, which is identical to the longer cycling life of the Al/Al cell employing AUdF. Although the CE obtained in AUdF still needs further improvement for practical use, this result reveals the feasibility of improving the reversibility of Al stripping/plating via electrolyte engineering. To understand the mechanism behind the improved electrochemical performance, electrochemical impedance spectroscopy (EIS) was applied to the Al/Al cells with AU and AUdF electrolytes. EIS spectra obtained after 15 cycles (at 0.054 mA cm^2) are shown in Figure 2d. In general, one depressed semicircle was observed for both cells, which can be well fitted with the equivalent circuit shown in Table S2 (Supporting Information). The fit results of the EIS data using the equivalent circuit are displayed in Table S2 (Supporting Information). The high-frequency intercept corresponds to a pure resistor (R_s) mainly associated with the bulk resistance of the electrolyte. AUdF-based Al/Al cell presents a lower R_s due to the higher ionic conductivity of AUdF with respect to AU. The semicircle is fitted with a constant phase element and a resistor (R_1) in parallel. The value of R_1 for the AUdF-based cell is only one fifth of that for the AU-based one. Since the dynamic equilibrium of the ions in the electrolytes are not affected by the addition of dFBn, the rather different resistance most likely originates from the SEI on AMAs. Therefore, the improved ionic conductivity and, particularly, the lowered SEI resistance via the addition of dFBn is the reason for the decreased polarization of AMAs.

Afterward, the morphology and SEI species on the surface of AMAs unmounted from Al/Al cells after cycling for 200 h were characterized by scanning electronic microscopy (SEM) and X-ray photoelectron spectroscopy (XPS), respectively. **Figure 3**a shows the typical texture of Al metal foil. After cycling for 200 h, the surface of both electrodes presents uneven morphology due to the repeated stripping/plating of Al (Figure 3b,c and Figure S7, Supporting Information). However, the electrode tested with AUdF exhibited a substantially flatter surface than that tested with AU. For instance, an Al deposit with a diameter of ≈60 µm was observed on the sample cycled in AU (Figure 3b), which could cause the cell's short circuit when penetrating through the separator as it occurred for the Al/AU/Al cell shown in Figure 2c. Therefore, the introduction of dFBn promotes a more homogeneous Al stripping/plating improving the cycling stability of AMAs.

Figure 3d–i and Figure S8 (Supporting Information) display the XPS spectra of the cycled AMAs unmounted from Al/Al cells employing AU or AUdF as the electrolyte. The peak located at around 400 eV in the N 1s spectra (Figure 3d,g) is assigned to the C–N bond of urea. In the Al 2p spectra (Figure 3e,h), two pairs of peak doublets are observed at 72.1 and 75.0 eV. The former one corresponds to metallic Al, while the other one can be assigned to the SEI species including Al_2O_3, Al–Cl, and Al–F.[51] The observation of a strong Al^0 peak indicates that the thickness of SEI is lower than the detection depth of the XPS, i.e., lower than 10 nm. Comparing the peak intensity of C–N in N 1s spectra and Al_2O_3/Al–Cl/Al–F in Al 2p spectra with that of the Al^0 in the Al 2p spectra, one can find that the electrode tested in AUdF exhibited more metallic Al and more C–N, suggesting that dFBn leads to a thinner SEI and promotes the contribution of urea to the SEI formation. The highest concentration of Al–Cl species and Al_2O_3 in the SEIs formed in AU is also evidenced by the results of the Cl 2p (Figure 3f,i) and O 1s regions (Figure S8b, Supporting Information). Finally, similar signals were observed in the F 1s spectra of the electrodes tested in AU and AUdF (Figure S8c, Supporting Information). These signals originate from the slight corrosion of the PTFE cell body by the electrolytes as PTFE is the only fluorine source in these cells.

These results demonstrate that the added dFBn increases the contribution of urea to the SEI formation while it mitigates the deposition of Al–Cl species, leading to relatively thinner SEI and consequently contributing to the promoted electrochemical performance of AMAs.

2.3. Electrochemical Performance and Interfacial Properties of Graphite Cathodes in AUdF

Graphite, relying on the highly reversible and fast de-/intercalation of $AlCl_4^-$, is certainly the most mature cathode of AMBs featuring excellent cyclic stability in IL-based electrolytes.[4,52,53] DELEs are also reported as the low-cost electrolytes for Al-graphite batteries, but their sluggish ion transport limits the rate capability of the cells and results in high cell polarization. However, the introduction of dFBn significantly promotes the ionic transport in the electrolyte bulk; hence, the developed electrolyte, i.e., AUdF, is expected to address this issue. To evaluate the influence of the dFBn co-solvent on the electrochemical performance of graphite cathodes, a commercial graphite was adopted as exhibited in Figure S9

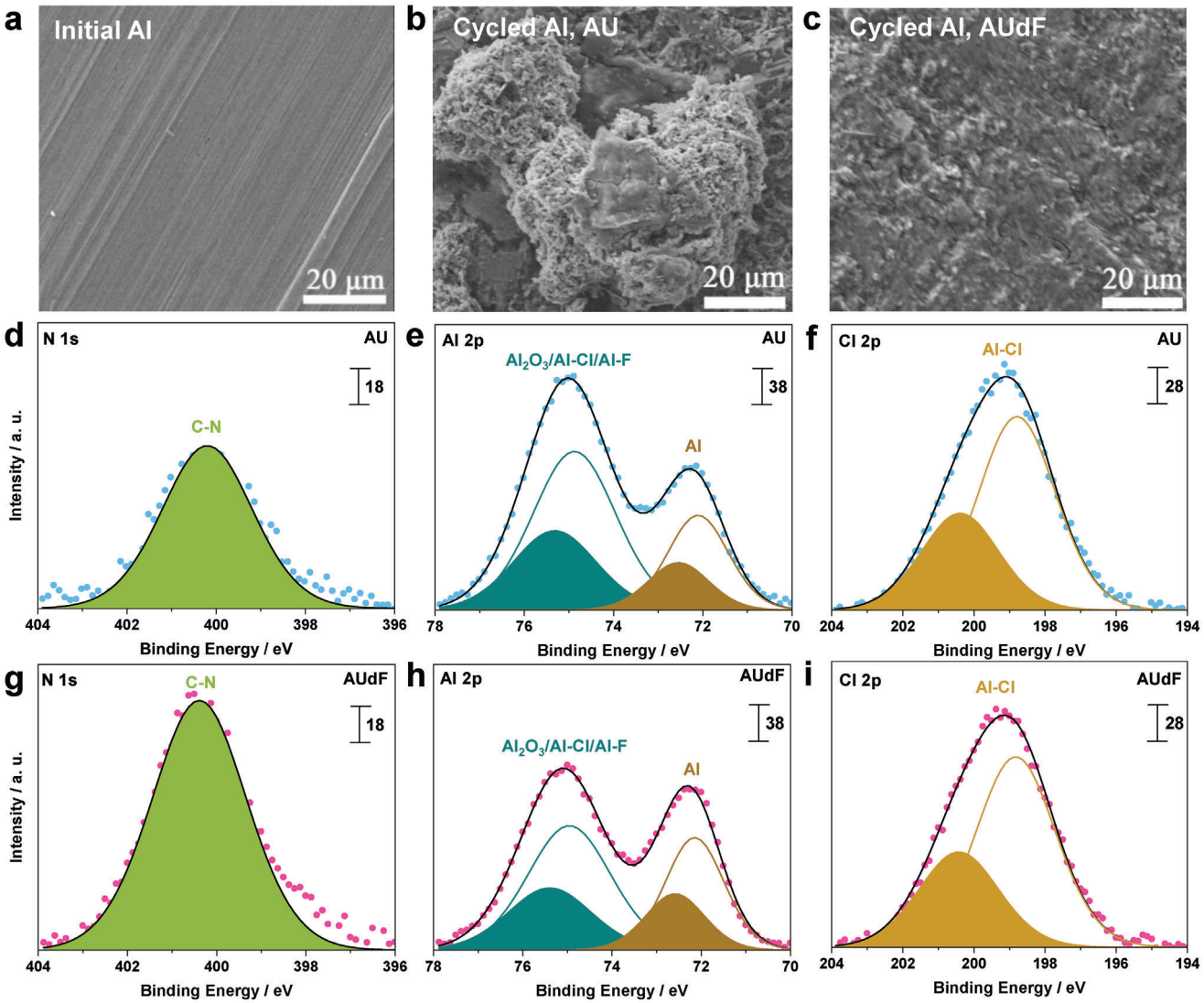

Figure 3. SEM images of a) polished aluminum foil and AMAs cycled in b) AU and c) AUdF. XPS detail spectra of d,g) N 1s, e,h) Al 2p, and f,i) Cl 2p regions of the AMAs cycled in AU and AUdF.

(Supporting Information). Specifically, three-electrode T-shaped cells employing graphite electrodes as working electrode, Al foils as counter and reference electrodes, and AU or AUdF as electrolyte were assembled and tested at 20 °C. The mass loading of graphite was 2.5 mg cm^{-2}. More details can be found in the Experimental Section in Supporting Information.

To validate the electrochemical activity of graphite cathodes in the electrolytes, cyclic voltammetry (CV) was performed. Figure S10 (Supporting Information) displays the CV curves with a scan rate of 2.0 mV s^{-1} in the 0.5–2.25 V (vs Al^{3+}/Al) potential window. A series of redox peaks overlapping with each other is observed in both electrolytes, demonstrating the electrochemical activity of graphite in these two electrolytes. Compared with the AU-based cell, however, the AUdF-based cell showed higher electrochemical activity.

The rate capability of the graphite cathode in the electrolytes was evaluated via galvanostatic cycling with potential limitations at various specific currents from 0.1 to 1.0 A g^{-1}. The dis-/charge profiles at different specific currents are compared in **Figure** 4a and Figure S11 (Supporting Information). For the AUdF-based cell, a flat voltage plateau following the slope below 2.0 V versus Al^{3+}/Al was observed upon charging, resulting in a reversible specific capacity of 75 mAh g^{-1}. When AU was employed, the platform at higher potential did not appear due to the high polarization, leading to a lower specific capacity (≈48 mAh g^{-1}). These results match well with those of the CV tests. The average potential upon discharge and charge of the cells at different specific currents is shown in Figure S12 (Supporting Information), while the difference between average charge and discharge potentials (ΔV, as an indicator for the internal resistance of the cell or the polarization voltage drop)[54] is summarized in Figure 4b. As the current density increases, ΔV shows an upward trend for both electrolytes, but the value for the AU-based cell is approximately twice that of the AUdF-based cell. Specifically, the Al-graphite cell

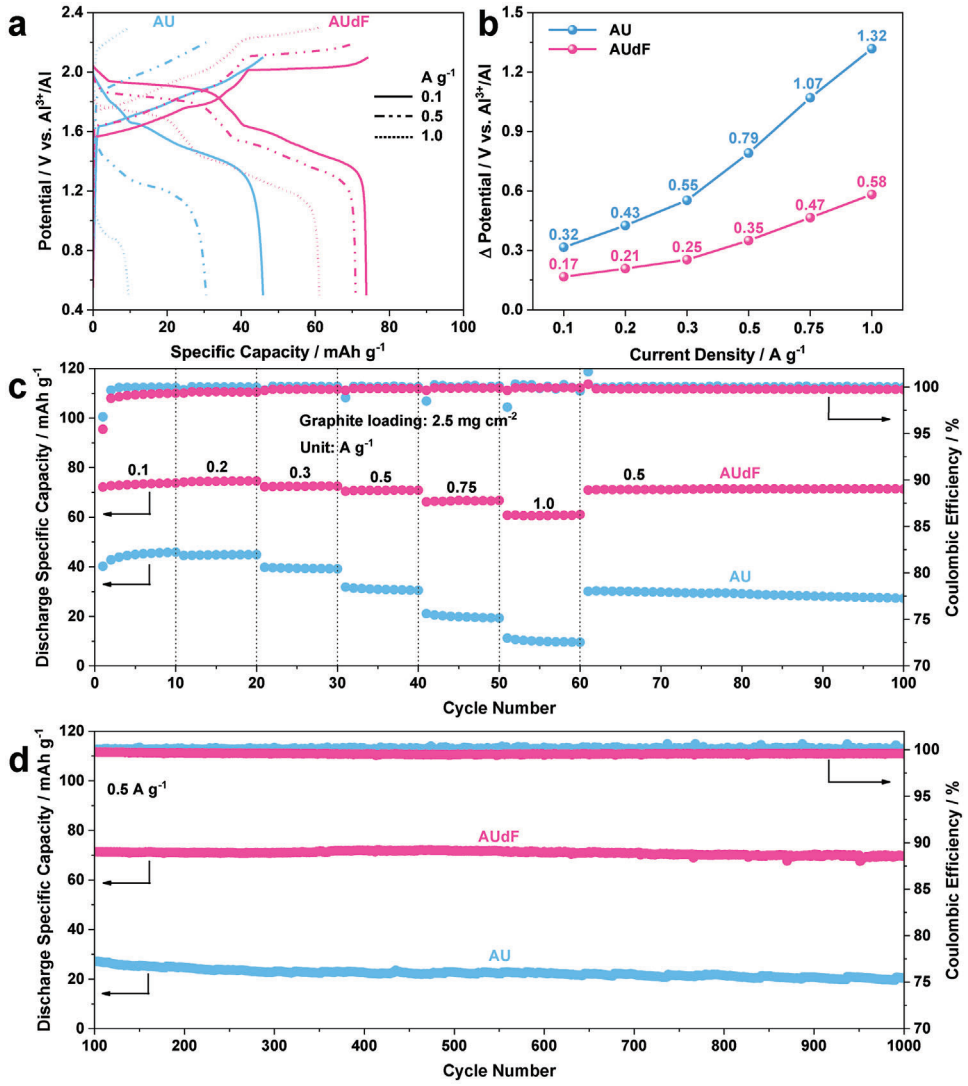

Figure 4. Comparison of electrochemical performance of Al-graphite cells employing AU and AUdF as electrolyte at 20 °C. a) Dis-/charge profiles at 0.1, 0.5, and 1.0 A g^{-1}. b) Difference between average charge and discharge potentials at different specific currents. Evolution of discharge specific capacity and Coulombic efficiency at c) different current rates and d) upon extended cycling at 0.5 A g^{-1}.

employing AUdF displayed ΔV of 0.17, 0.35, and 0.58 V at 0.1, 0.5, and 1 A g^{-1}, respectively. In contrast, the ΔV of the same cell employing AU was 0.32, 0.79, and 1.32 V, respectively. Additionally, an AU-based Al-graphite battery tested with different charge cut-off voltages (2.1, 2.15, 2.2, 2.3, and 2.4 V) at 0.1 A g^{-1} and 20 °C as shown in Figure S13 (Supporting Information), displayed a comparable performance with previous literature when the charge cut-off voltage was set to 2.4 V.[31]

The evolution of discharge specific capacity of Al-graphite cells employing the AU and AUdF are compared in Figure 4c. Due to the rapidly growing over-voltage upon increasing current rates, the specific capacity dropped from 46 mAh g^{-1} at 0.1 A g^{-1} to 10 mAh g^{-1} at 1 A g^{-1} when AU was used as the electrolyte. On the contrary, the AUdF-based cell with a discharge specific capacity of 74 mAh g^{-1} at 0.1 A g^{-1} still delivered 61 mAh g^{-1} at 1 A g^{-1}. These results demonstrate that the addition of dFBn can effectively decrease the polarization of both the graphite cathode and the AMA, consequently promoting the rate capability.

Following the test of rate capability, the cells were subjected to long-term cycling at 0.5 A g^{-1}. The evolution of the discharge specific capacity and CE during these tests is presented in Figure 4d. Both cells exhibited a steady capacity, however, the AUdF-based cell achieved a substantially higher discharge specific capacity of 70 mAh g^{-1} compared with 21 mAh g^{-1} for the AU-based cell at the 1000th cycle. Furthermore, the degree of polarization was obviously mitigated by dFBn according to the potential profiles at various cycles shown in Figure S14 (Supporting Information) and the average dis-/charge potential shown in Figure S15 (Supporting Information). The same remarkable improvement was also observed upon long-term cycling tests at 0.5 A g^{-1} of the cells within the cut-off potential of 0.5–2.25 V (Figure S16, Supporting Information). After 500 cycles, the AUdF-based cell presented a

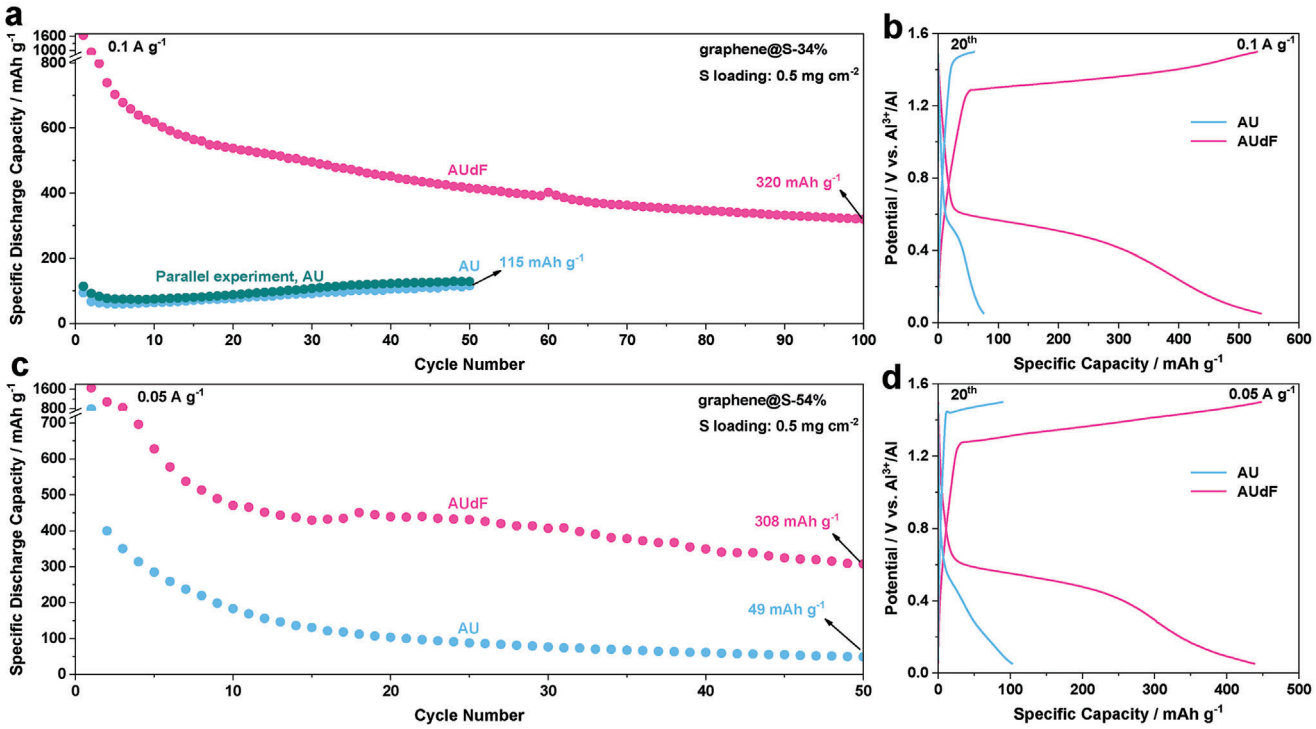

Figure 5. Electrochemical performance of Al-S cells based on a,b) graphene@S-34% and c,d) graphene@S-54% at 20 °C. Evolution of specific discharge capacity upon cycling at 0.1 A g^{-1} (a) and 0.05 A g^{-1} (c). Potential profiles in the 20th dis-/charge cycle (b, d).

discharge specific capacity of 71 mAh g^{-1}, while only 31 mAh g^{-1} were delivered by the AU-based cell.

To investigate the reasons for the reduced polarization achieved by dFBn addition, EIS spectra were measured on the graphite cathodes in AU and AUdF after 20 cycles (Figure S17, Supporting Information). As expected, the higher ionic conductivity of AUdF lead to a smaller intercept at high frequencies. Additionally, the depressed semicircle is smaller for AUdF than AU. To understand the origin of this difference, graphite electrodes were further examined with SEM, energy dispersive -X-ray spectroscopy (EDX), and XPS after 200 cycles of dis-/charge at 0.5 A g^{-1} in the two electrolytes. As observed via SEM and EDX (Figure S18, Supporting Information), the morphology of the cathode cycled in AUdF displays a porous structure, and elemental composition did not show distinct differences. The chemical state of the species on the cycled electrodes was also examined via XPS (Figure S19, Supporting Information). The spectra do not reveal distinguishable differences, which indicates that the cathode/electrolyte interphase (CEI) on the graphite cathodes is very similar in AU and AUdF electrolyte. Therefore, the CEIs generated on graphite electrodes in these two electrolytes are not responsible for the different size of the depressed semicircle observed in EIS spectra. Instead, considering the viscosity of the electrolytes (Figure 1a) and the porous nature of the graphite electrodes (Figure S18, Supporting Information), one may infer that the reduced resistance of the depressed semicircle originates from the promoted wettability of the electrolyte toward the graphite electrode. Although further investigation is required, these results have clearly demonstrated the beneficial effect of dFBn co-solvents on reducing the polarization of Al-graphite cells based on DELEs.

2.4. Electrochemical Performance of Sulfur Cathodes in AUdF

Sulfur is a promising cathode candidate for AMBs due to its low cost and high theoretical specific capacity.[55–57] Recently, Al-S batteries have made significant progress, mainly with imidazole-based ionic liquid electrolytes.[58–63] Al-S batteries employing low-cost urea or urea-derivatives-based electrolytes usually exhibit poor cycling ability,[30,36,64] due to the high viscosity and/or low ionic conductivity of the electrolyte, etc.[36]

LC-DELE, however, appears a promising electrolyte for Al-S batteries. Therefore, three-electrode T-shaped Al-S cells employing sulfur electrodes as the working electrode, Al metal as the counter and reference electrodes, and AU or AUdF as the electrolyte were assembled and tested at 20 °C. Graphene (Figures S20b,S21, Supporting Information) was selected as the sulfur host, and the sulfur content of the composite was 34 or 54 wt% as examined with TGA (Figure S22, Supporting Information). The loading of sulfur was set to 0.5 mg cm^{-2}. More details can be found in the Experimental Section of the Supporting Information.

Figure 5a shows the discharge specific capacity evolution of Al-S cells employing graphene@S (34 wt%) cathode and AU or AUdF electrolyte at 0.1 A g^{-1}. The potential profiles at the 1st cycle are displayed in Figure S23 (Supporting Information). The AUdF-based Al-S cell delivered an initial discharge specific capacity of 1640 mAh g^{-1}, which is close to the theoretical capacity.

After cycling for 100 cycles, 320 mAh g^{-1} was still delivered. In contrast, the AU-based cell displayed, in duplicate experiments, an initial discharge specific capacity of 94 mAh g^{-1}, reaching 115 mAh g^{-1} after 50 cycles. From the potential profiles, a severe polarization is observed for the AU-based cell in the 1st cycle, which is greatly reduced for AUdF, i.e., by the addition of dFBn. Such polarization reduction was observed at various cycles as shown in Figure S23 (Supporting Information). The CV curves (Figure S24, Supporting Information) of the AUdF-based Al-S cell show a larger area and more prominent redox peaks compared with AU, which agrees with the potential profiles in Figure 5b.

Figure 5c presents the discharge specific capacity evolution of sulfur cathodes with higher sulfur content (54%), but same sulfur loading (0.5 mg cm^{-2}) upon cycling at 0.05 A g^{-1}. The first cycle potential profile of the cells employing such a cathode and AU or AUdF as electrolyte are displayed in Figure S25 (Supporting Information). Keeping the sulfur loading fixed, i.e., 0.5 mg cm^{-2}, the electrode employing graphene@S-54% exhibited a lower overall electrode areal loading and thickness. As a result, the graphene@S-54% electrode exhibited a higher initial specific capacity of 798 mAh g^{-1} with AU than the graphene@S-34% one.[36] Despite the promoted initial specific capacity, the AU-based cell exhibited a fast capacity fading to 49 mAh g^{-1} after 50 cycles. As AUdF exhibited a much lower viscosity than AU, the initial specific capacity was not influenced by the sulfur content in the graphene@S composite. However, more pronounced potential plateaus were observed during charge and discharge of the cell (Figure 5d and Figure S25, Supporting Information). After 50 dis-/charge cycles, a high specific capacity of 308 mAh g^{-1} was still delivered.

The sulfur cathodes were characterized after 20 cycles in AU and AUdF with SEM and EDX. Despite a rather similar surface morphology (Figure S26a,b, Supporting Information), the EDX spectra comparison (Figure S26c, Supporting Information) showed a less intense sulfur peak for the electrode cycled in AUdF. Considering this and the lower specific capacity obtained in AU, one can infer that the improved fluidity of the electrolyte after dFBn addition results in its better infiltration into the composite sulfur cathode and, consequently, a better sulfur utilization. This led to higher specific capacity and less residual sulfur in the cathode, since its activity led to a larger generation of polysulfides dissolving into in AUdF.

Although the polarization of Al-S battery has been significantly reduced through the electrolyte optimization, it cannot be ignored that the cell polarization is still large. The introduction of functional catalysts in the cathode and/or the separator may promote the polysulfides conversion.[58,63,65] The combination of these latter approaches and the electrolyte designed in this work is expected to further reduce the cell polarization.

3. Conclusions

LC-DELEs constructed via diluting DELEs, i.e., AU, with non-solvating co-solvent, i.e., dFBn, have been developed for AMBs. By the addition of dFBn, the fluidity and ionic conductivity of AU are effectively improved without affecting its ionic dynamics. Due to a better infiltration of AUdF into the porous cathodes, promoting ion transport, cells employing either graphite or sulfur cathodes exhibited reduced polarization and promoted specific capacity. Moreover, dFBn also modified the SEI on AMAs reducing their interfacial resistance, which, together with the higher electrolyte's ionic conductivity, led to reduced polarization, improved rate capability, and enhanced reversibility of AMAs. Summarizing, adding non-solvating co-solvents into DELEs to construct LC-DELEs provides a new path to develop low-cost AMBs with high energy and/or power density.

Supporting Information

Supporting Information is available from the Wiley Online Library or from the author.

Acknowledgements

C.X. and X.L. gratefully acknowledge the financial support from the China Scholarship Council (CSC). All authors acknowledge the basic support of the Helmholtz Association.

Open access funding enabled and organized by Projekt DEAL.

Conflict of Interest

The authors declare no conflict of interest.

Data Availability Statement

The data that support the findings of this study are available on request from the corresponding author. The data are not publicly available due to privacy or ethical restrictions.

Keywords

aluminum graphite batteries, aluminum sulfur batteries, deep eutectic solvents, locally concentrated electrolytes, non-solvating co-solvents

Received: January 6, 2024
Revised: February 14, 2024
Published online: March 6, 2024

[1] K. L. Ng, B. Amrithraj, G. Azimi, *Joule* **2022**, *6*, 134.
[2] M. Jiang, C. Fu, P. Meng, J. Ren, J. Wang, J. Bu, A. Dong, J. Zhang, W. Xiao, B. Sun, *Adv. Mater.* **2022**, *34*, 2102026.
[3] G. A. Elia, K. V. Kravchyk, M. V. Kovalenko, J. Chacón, A. Holland, R. G. A. Wills, *J. Power Sources* **2021**, *481*, 228870.
[4] M. C. Lin, M. Gong, B. Lu, Y. Wu, D. Y. Wang, M. Guan, M. Angell, C. Chen, J. Yang, B. J. Hwang, H. Dai, *Nature* **2015**, *520*, 324.
[5] D. Ma, D. Yuan, C. Ponce de León, Z. Jiang, X. Xia, J. Pan, *Energy Environ. Mater.* **2023**, *6*, e12301.
[6] E. Faegh, B. Ng, D. Hayman, W. E. Mustain, *Nat. Energy* **2021**, *6*, 21.
[7] Z. Yuan, Q. Lin, Y. Li, W. Han, L. Wang, *Adv. Mater.* **2023**, *35*, 2211527.
[8] C. Xu, T. Diemant, X. Liu, S. Passerini, *Adv. Funct. Mater.* **2023**, *33*, 2214405.
[9] J. Wang, J. Tu, C. Chang, H. Zhu, *J. Power Sources* **2021**, *492*, 229674.
[10] Y. Du, B. Zhang, R. Kang, W. Zhou, W. Zhang, H. Jin, J. Wan, J. Zhang, G. Chen, *Inorg. Chem. Front.* **2022**, *9*, 925.

[11] J. Zhang, L. Zhang, Y. Zhao, J. Meng, B. Wen, K. M. Muttaqi, M. R. Islam, Q. Cai, S. Zhang, *Adv. Energy Mater.* **2022**, *12*, 2200959.
[12] L. Xing, K. A. Owusu, X. Liu, J. Meng, K. Wang, Q. An, L. Mai, *Nano Energy* **2021**, *79*, 105384.
[13] H. Zhang, Y. Liu, L. Yang, L. Zhao, X. Dong, H. Wang, Y. Li, T. Sun, Q. Li, H. Li, *Energy Storage Mater.* **2022**, *47*, 336.
[14] Y. Tong, A. Gao, Q. Zhang, T. Gao, J. Yue, F. Meng, Y. Gong, S. Xi, Z. Lin, M. Mao, S. Peng, X. Wang, D. Xiao, D. Su, Y. Luo, H. Li, L. Chen, L. Suo, L. Gu, *Energy Storage Mater.* **2021**, *37*, 87.
[15] R. Kang, Y. Du, W. Zhou, D. Zhang, W. Zhang, J. Wan, G. Chen, J. Zhang, *ACS Appl. Energy Mater.* **2022**, *5*, 10287.
[16] Z. Lin, M. Mao, C. Yang, Y. Tong, Q. Li, J. Yue, G. Yang, Q. Zhang, L. Hong, X. Yu, L. Gu, Y. S. Hu, H. Li, X. Huang, L. Suo, L. Chen, *Sci. Adv.* **2021**, *7*, 6314.
[17] G. Du, H. Pang, *Energy Storage Mater.* **2021**, *36*, 387.
[18] Y. Du, B. Zhang, W. Zhang, H. Jin, J. Qin, J. Wan, Y. Zhang, Z. Wang, J. Zhang, G. Chen, *J. Alloys Compd.* **2022**, *896*, 162901.
[19] Z. Wang, X. Zheng, A. Chen, Y. Han, L. Wei, J. Li, *ACS Mater. Lett.* **2022**, *4*, 1436.
[20] L. Yao, S. Ju, T. Xu, W. Wang, X. Yu, *ACS Nano* **2023**, *17*, 25027.
[21] G. Wang, E. Dmitrieva, B. Kohn, U. Scheler, Y. Liu, V. Tkachova, L. Yang, Y. Fu, J. Ma, P. Zhang, F. Wang, J. Ge, X. Feng, *Angew. Chem., Int. Ed.* **2022**, *61*, e202116194.
[22] X. Han, S. Li, W. L. Song, N. Chen, H. Chen, S. Huang, S. Jiao, *Adv. Energy Mater.* **2021**, *11*, 2101446.
[23] H. Lei, J. Tu, W. L. Song, H. Jiao, X. Xiao, S. Jiao, *Inorg. Chem. Front.* **2021**, *8*, 1030.
[24] W. Lv, G. Wu, X. Li, J. Li, Z. Li, *Energy Storage Mater.* **2022**, *46*, 138.
[25] T. Zhang, T. Cai, W. Xing, T. Li, B. Liang, H. Hu, L. Zhao, X. Li, Z. Yan, *Energy Storage Mater.* **2021**, *41*, 667.
[26] Z. Li, W. Lv, G. Wu, W. Zhang, *Electrochim. Acta* **2021**, *401*, 139498.
[27] J. Zheng, H. Zhang, T. Xu, S. Ju, G. Xia, X. Yu, *Adv. Funct. Mater.* **2023**, *34*, 2307486.
[28] Q. Pang, J. Meng, S. Gupta, X. Hong, C. Y. Kwok, J. Zhao, Y. Jin, L. Xu, O. Karahan, Z. Wang, S. Toll, L. Mai, L. F. Nazar, M. Balasubramanian, B. Narayanan, D. R. Sadoway, *Nature* **2022**, *608*, 704.
[29] P. Almodóvar, D. Giraldo, C. Díaz-Guerra, J. Ramírez-Castellanos, J. M. González Calbet, J. Chacón, M. L. López, *J. Power Sources* **2021**, *516*, 230656.
[30] H. Li, R. Meng, Y. Guo, B. Chen, Y. Jiao, C. Ye, Y. Long, A. Tadich, Q. H. Yang, M. Jaroniec, S. Z. Qiao, *Nat. Commun.* **2021**, *12*, 5714.
[31] H. Jiao, C. Wang, J. Tu, D. Tian, S. Jiao, *Chem. Commun.* **2017**, *53*, 2331.
[32] G. Zhu, M. Angell, C. J. Pan, M. C. Lin, H. Chen, C. J. Huang, J. Lin, A. J. Achazi, P. Kaghazchi, B. J. Hwang, H. Dai, *RSC Adv.* **2019**, *9*, 11322.
[33] J. Tu, W. L. Song, H. Lei, Z. Yu, L. L. Chen, M. Wang, S. Jiao, *Chem. Rev.* **2021**, *121*, 4903.
[34] M. Angell, C. J. Pan, Y. Rong, C. Yuan, M. C. Lin, B. J. Hwang, H. Dai, *Proc. Natl. Acad. Sci. U. S. A.* **2017**, *114*, 834.
[35] M. Angell, G. Zhu, M. C. Lin, Y. Rong, H. Dai, *Adv. Funct. Mater.* **2020**, *30*, 1901928.
[36] J. Lampkin, H. Li, L. Furness, R. Raccichini, N. Garcia-Araez, *ChemSusChem* **2020**, *13*, 3514.
[37] C. Zhu, C. Sun, R. Li, S. Weng, L. Fan, X. Wang, L. Chen, M. Noked, X. Fan, *ACS Energy Lett.* **2022**, *7*, 1338.
[38] Y. R. Tsai, B. Vedhanarayanan, T. Y. Chen, Y. C. Lin, J. Y. Lin, X. Ji, T. W. Lin, *J. Power Sources* **2022**, *521*, 230954.
[39] W. Dean, M. Muñoz, J. Noh, Y. Liang, W. Wang, B. Gurkan, *Electrochim. Acta* **2023**, *474*, 143517.
[40] W. Yang, X. Du, J. Zhao, Z. Chen, J. Li, J. Xie, Y. Zhang, Z. Cui, Q. Kong, Z. Zhao, C. Wang, Q. Zhang, G. Cui, *Joule* **2020**, *4*, 1557.
[41] X. Xiao, J. Tu, Z. Huang, S. Jiao, *Phys. Chem. Chem. Phys.* **2021**, *23*, 10326.
[42] J. Zheng, S. Chen, W. Zhao, J. Song, M. H. Engelhard, J. G. Zhang, *ACS Energy Lett.* **2018**, *3*, 315.
[43] S. Lee, K. Park, B. Koo, C. Park, M. Jang, H. Lee, H. Lee, *Adv. Funct. Mater.* **2020**, *30*, 2003132.
[44] X. Liu, A. Mariani, M. Zarrabeitia, M. E. Di Pietro, X. Dong, G. A. Elia, A. Mele, S. Passerini, *Energy Storage Mater.* **2022**, *44*, 370.
[45] S. Chen, J. Zheng, D. Mei, K. S. Han, M. H. Engelhard, W. Zhao, W. Xu, J. Liu, J. G. Zhang, *Adv. Mater.* **2018**, *30*, 1706102.
[46] X. Liu, A. Mariani, T. Diemant, X. Dong, P. H. Su, S. Passerini, *Angew. Chem., Int. Ed.* **2023**, *135*, e202305840.
[47] X. Liu, A. Mariani, H. Adenusi, S. Passerini, *Angew. Chem., Int. Ed.* **2023**, *62*, e202219318.
[48] W. Cai, Y. Deng, Z. Deng, Y. Jia, Z. Li, X. Zhang, C. Xu, X. Q. Zhang, Y. Zhang, Q. Zhang, *Adv. Energy Mater.* **2023**, *13*, 2301396.
[49] L. Qin, N. Xiao, J. Zheng, Y. Lei, D. Zhai, Y. Wu, *Adv. Energy Mater.* **2019**, *9*, 1902618.
[50] P. W. A. Willems, W. Peter Vandertop, R. M. Verdaasdonk, C. F. P. Van Swol, G. H. Jansen, *Lasers Surg. Med.* **2001**, *28*, 324.
[51] W. Li, C. Y. Cao, L. Y. Wu, M. F. Ge, W. G. Song, *J. Hazard. Mater.* **2011**, *198*, 143.
[52] X. Zheng, F. Zhao, L. Ma, R. Tang, Y. Dong, G. Kong, Y. Zhang, S. Niu, G. Tang, Y. Wang, A. Pang, W. Li, L. Wei, *Electrochim. Acta* **2021**, *380*, 138201.
[53] C. Xu, W. Zhang, P. Li, S. Zhao, Y. Du, H. Jin, Y. Zhang, Z. Wang, J. Zhang, *Sustain. Energy Fuels* **2019**, *4*, 121.
[54] C. P. Aiken, J. E. Harlow, R. Tingley, T. Hynes, E. R. Logan, S. L. Glazier, A. S. Keefe, J. R. Dahn, *J. Electrochem. Soc.* **2020**, *167*, 130541.
[55] M. Klimpel, M. V. Kovalenko, K. V. Kravchyk, *Commun. Chem.* **2022**, *5*, 77.
[56] Q. Zhou, Y. Wu, J. Gautam, D. Wang, X. Jiang, Z. Ma, H. Zhang, L. Ni, G. Diao, *Coord. Chem. Rev.* **2023**, *474*, 214856.
[57] Z. Huang, S. Li, Z. Wang, W. Wang, H. Lei, S. Jiao, *Adv. Energy Mater.* **2023**, *13*, 2302464.
[58] S. Ju, J. Ye, H. Zhang, W. Wang, G. Xia, W. Cui, Y. Yang, H. Pan, X. Yu, *Energy Storage Mater.* **2023**, *56*, 1.
[59] X. Zheng, Z. Wang, J. Li, L. Wei, *Sci. China Mater.* **2022**, *65*, 1463.
[60] Y. Ai, S.-C. Wu, F. Zhang, X. Zhang, R. Li, Y. Lan, L. Cai, W. Wang, *Energy Storage Mater.* **2022**, *48*, 297.
[61] R. Jay, A. L. Jadhav, L. W. Gordon, R. J. Messinger, *Chem. Mater.* **2022**, *34*, 4486.
[62] Y. Zhang, L. Ma, R. Tang, X. Zheng, X. Wang, Y. Dong, G. Kong, F. Zhao, L. Wei, *Int. J. Hydrogen Energy* **2021**, *46*, 4936.
[63] C. Xu, M. Zarrabeitia, Y. Li, J. Biskupek, U. Kaiser, X. Liu, S. Passerini, *ACS Nano* **2023**, *17*, 25234.
[64] D. Zhang, W. Chu, D. Y. Wang, S. Li, S. Zhao, X. Zhang, Y. Fu, H. Yu, *Adv. Funct. Mater.* **2022**, *32*, 2205562.
[65] C. Xu, T. Diemant, A. Mariani, M. Pietro, A. Mele, X. Liu, S. Passerini, *Angew. Chem., Int. Ed.* **2024**, *63*, e202318204.